Available online at www.sciencedirect.com
ScienceDirect
Journal of Physics and Chemistry of Solids 68 (2007) 1630–1642
JOURNAL OF PHYSICS AND CHEMISTRY OF SOLIDS
www.elsevier.com/locate/jpcs

An atypical coordination in hexacyanometallates: Structure and properties of hexagonal zinc phases

J. Rodríguez-Hernández[a], E. Reguera[a,b,*], E. Lima[c], J. Balmaseda[a,d], R. Martínez-García[a], H. Yee-Madeira[e]

[a]*Institute of Science and Technology of Materials, University of Havana, 10400 Havana, Cuba*
[b]*Center of Applied Science and Advanced Technologies of IPN, Legaria 694, Col. Irrigación, C.P. 11500, México, D.F., Mexico*
[c]*Metropolitan Autonomous University, Iztapalapa, Mexico, D.F., Mexico*
[d]*Institute of Materials Research, National Autonomous University, México, D.F., Mexico*
[e]*School of Physics and Mathematics of IPN, Mexico, D.F., Mexico*

Received 20 January 2007; received in revised form 16 March 2007

Abstract

In hexacyanometallates, the involved transition metals are usually found with octahedral coordination. The exception corresponds to the hexagonal zinc phases where this metal appears tetrahedrally coordinated to N ends from the CN ligands. Those zinc hexacyanometallates where such atypical coordination appears were identified and for four of them the crystal structure was refined from X-ray diffraction powder patterns using the Rietveld method. Zinc hexacyanoferrates (III), hexacyanocobaltate (III), hexacyanoiridate (III) and the mixed zinc–cesium hexacyanoferrate (II) were found to be dimorphic, cubic (Fm-3m) and hexagonal (R-3c), related to the zinc atom in octahedral or tetrahedral coordination, respectively. In the absence of an exchangeable cation, the hexagonal phases result anhydrous. This last feature was attributed to a low polar character for the pores surface. The Mössbauer spectrum of hexagonal zinc hexacyanoferrate (III) is an unresolved quadrupole splitting doublet ($\Delta = 0.18$ mm/s). The iron nucleus is sensing a weak electric field gradient related to a relatively high symmetry for its ligands and charge environment. The IR spectrum appears to be an excellent sensor to identify the coordination for the zinc atom in a given sample. For the tetrahedral coordination, the CN stretching absorption was found at least 8 cm^{-1} above the frequency observed for this vibration in the octahedral one. For hydrated phases, the crystal water evolves on heating preserving the material porous framework. The temperature at which the material becomes anhydrous parallels the polarizing power of the charge balancing cation sited within the channels. Hexagonal Zn–Cs ferrocyanide becomes anhydrous at 100 °C, while for the Zn–Na analogue a heating close to 200 °C is required. The stability temperature range for the anhydrous phases depends on the nature of the engaged hexacyanometallate anion; the higher stability was observed for hexacyanoferrates (II). Zinc ferricyanide shows the weaker magnetic interaction for the hexagonal modification due to an unfavourable geometry for the overlapping path between the unpaired electrons on the iron(III) atoms. The open 3D porous network is formed by relatively large ellipsoidal cavities, three per cell, communicated through elliptical openings (windows), six per cavity. For dimorphic zinc hexacyanometallates (III), the most compact structure (higher density) corresponds to the hexagonal modification, however, it has the largest cavity windows and cavity (pore) size, and also the higher thermal stability.

Keywords: A. Inorganic compounds; A. Microporous materials; C. Mössbauer spectroscopy; C. X-ray diffraction; D. Crystal structure

1. Introduction

Transition metal hexacyanometallates, commonly known as Prussian blue analogues, usually have an open-channel framework appropriate for small molecules separation and storage [1–5]. Recent studies have reported their potentiality for hydrogen storage [6–9].

*Corresponding author. Institute of Science and Technology of Materials, University of Havana, 10400 Havana, Cuba.
Tel.: +53 573 2096653; fax: +53 573 2096653.
E-mail address: ereguera@yahoo.com (E. Reguera).

0022-3697/$ - see front matter © 2007 Elsevier Ltd. All rights reserved.
doi:10.1016/j.jpcs.2007.03.054

The possibilities of these materials as molecular sieves [10], for $^{137}Cs^{+}$ removal from radioactive waste solutions [11], in some catalytic processes [12,13], and for therapy of animals and humans affected by nuclear accidents [14], are also known. All these potential applications are related to their crystal structure which is known for only a few compositions. In turn, the crystal structure is closely related to the coordination adopted by the metal centres.

In hexacyanometallates, the involved transition metals are usually found with octahedral coordination, crystallizing, with some exceptions, within the cubic unit cell (Fm-3m), typical of Prussian blue analogues [15]. Some zinc hexacyanoferrates (II,III) have been reported as hexagonal where the Zn^{2+} atom is found tetrahedrally coordinated to four N atoms from CN ligands [16–19]. Such coordination provides a relatively high thermal stability to these materials and also an interesting porous framework because both metal centres have saturated their coordination sphere with atoms from the bridge group (–C≡N–). From these facts, we have explored the crystal structure of zinc hexacyanometallates in order to identify the occurrence of such coordination for the Zn^{2+} atom. The results obtained are reported in this contribution, including the refined crystal structure for four compositions. The structural study, from X-ray diffraction (XRD) data, was complemented with information from thermo-gravimetry (TG), IR, Mössbauer and magnetic measurements.

2. Experimental

Aqueous hot solutions (0.01 M) of Zn^{2+} chloride and $K_n{}^{+}[M(CN)_6]^{n-}$ where M = Cr^{III}, Mn^{III}, Fe^{II}, Fe^{III}, Co^{III}, Ir^{III} and Pt^{IV} were mixed and the resulting precipitate separated after 2 days of ageing at 60 °C within the mother liquor. The obtained solid was washed several times with distilled water in order to remove all the accompanying ions and then dried in air until it had constant weight. For Zn ferrocyanide, the solid precipitated from sodium ferrocyanide was also prepared. $K_n{}^{+}[M(CN)_6]^{n-}$ where M = Cr^{III}, Fe^{II}, Fe^{III}, Co^{III}, and Pt^{IV}, and Zn^{2+} chloride were Sigma-Aldrich reagents. $K_3[Ir(CN)_6]$ was provided by Alfa Aesar (a Johnson Matthey Co.). $K_3[Mn(CN)_6]$ was prepared *in situ* according to a reported synthetic route [20].

The nature of the obtained complex salts as hexacyanometallates was established from IR spectra. The metals atomic ratio in the studied samples was estimated from energy-dispersed spectroscopy (EDS) analyses, using a spectrometer (from Noran Co.) coupled to a SEM microscope (from Jeol Co.). The samples to be analysed were pressed and then coated with a thin film of an Au–Pt alloy. The EDS data were processed using a chemistry defined quantification method included in the equipment data processing software. The hydration degree (number of water molecules per formula unit) was estimated from the TG curves. Mixed compositions of Zn ferrocyanides with A = NH_4, Rb and Cs were prepared through ionic exchange from $Zn_3Na_2[Fe(CN)_6]_2 \cdot xH_2O$, in hot aqueous solutions, according to a reported procedure [18].

From trivalent complex anions, compounds of formula unit $Zn_3[M(CN)_6]_2 \cdot xH_2O$ (M = Cr, Mn, Fe, Co, Ir) were formed. Zinc ferricyanide, $Zn_3[Fe(CN)_6]_2 \cdot xH_2O$, has been reported to be dimorphic, cubic (Fm-3m) and hexagonal (R-3c) [19,21]. The cubic phase is usually obtained from the synthesis at room temperature, while the hexagonal one is formed from hot solutions or dehydrating the cubic phase by heating. From this fact, the possible formation of the hexagonal phase for the remaining zinc hexacyanometallates (III) was explored by means of a hydrothermal treatment in boiling water for at least 24 h and then the water evaporated at 80 °C up to dryness. In Table 1, the preparative route for all the studied samples, the estimated formula unit, and the samples label are indicated.

A high-resolution TA Instrument (Hi-ResTM) thermogravimetric analyser TGA 2950 and instrument control software Thermal Advantage version 1.1A were used to measure the weight loss profiles for the studied samples. The TGA 2950 was used in dynamic rate mode where the heating rate is varied dynamically according to a ramp in response to the derivative of weight change (as derivative increases, heating rate is decreased and vice versa). The heating rates were constrained to be in the 0.001–5 °C/min range with an instrumental resolution of 5. The furnace purge was nitrogen using flow rate of 100 mL/min. IR spectra were collected using an FT-IR spectrophotometer (Equinox 55 from Bruker) and the KBr pressed disk technique, except for ferricyanides which reduce on milling and pressing forming the mixed K ferrocyanide [22]. In this case, the IR spectra were run in Nujol mulls. IR spectra of mechanical mixtures of Zn ferro- and ferri-cyanide were also studied in order to estimate the fraction of ferrous species when it appears as impurity from the Zn ferricyanide synthesis. As sensor the integrated ν(CN) absorption was used. Mössbauer spectra were recorded at room temperature using a constant acceleration spectrometer (from Wissel) operated in the transmission mode and a ^{57}Co/Rh source. All the spectra were recorded under the thin absorbed condition and for at least one million of counts per channel. The obtained Mössbauer spectra were fitted using the *MossWinn* program [23] in order to obtain the values of isomer shift (δ), quadrupole splitting (Δ), linewidth (Γ) and relative sub-spectrum area (A). The value of δ is reported relative to sodium nitroprusside. Magnetic data were collected at low temperature using a SQUID magnetometer (Quantum Design MPMS XL7).

XRD powder patterns were recorded in Bragg–Brentano geometry by means of a D8 Advance diffractometer (from Bruker) and monochromatic Cu Kα radiation, from 5° to 110° (2θ), at a step size of 0.025 and 25 s of counting time. XRD powder patterns under vacuum (10^{-5} Torr) and at 77 K were collected at XPD beamline of the LNLS synchrotron radiation facility (at Campinas, Brazil) at a wavelength of 1.796760 Å, from 5° to 110° (2θ), and at a step size of 0.01. The patterns were indexed using the

Table 1
Sample designation, chemical formula and synthetic route for all the studied compositions

Sample designation	Sample formula unit	Sample synthetic route
$Zn_3Na_2Fe_2$–H	$Zn_3Na_2[Fe(CN)_6]_2 \cdot xH_2O$	Precipitation from 0.01 M aqueous hot solutions of $Na_4[Fe(CN)_6] \cdot xH_2O$ and $ZnCl_2$ and then aged for 2 days at 60 °C
$Zn_3K_2Fe_2$–H	$Zn_3K_2[Fe(CN)_6]_2 \cdot xH_2O$	Precipitation from 0.01 M aqueous hot solutions of $K_4[Fe(CN)_6] \cdot xH_2O$ and $ZnCl_2$ and then aged for 2 days at 60 °C
$Zn_3Rb_2Fe_2$–H	$Zn_3Rb_2[Fe(CN)_6]_2 \cdot xH_2O$	Ionic exchange from $Zn_3Na_2[Fe(CN)_6]_2 \cdot xH_2O$ in a hot solution of RbCl
$Zn_3(NH_4)2Fe_2$–H	$Zn_3(NH_4)_2[Fe(CN)_6]_2 \cdot xH_2O$	Ionic exchange from $Zn_3Na_2[Fe(CN)_6]_2 \cdot xH_2O$ in a hot solution of NH_4Cl
$ZnCs_2Fe$–C	$ZnCs_2[Fe(CN)_6]$	Precipitation from 0.01 M hot aqueous solutions of $K_4[Fe(CN)_6] \cdot xH_2O$, $ZnCl_2$ and CsCl and then aged for 2 days at 60 °C
$Zn_3Cs_2Fe_2$–H	$Zn_3Cs_2[Fe(CN)_6]_2 \cdot xH_2O$	Ionic exchange from $Zn_3Na_2[Fe(CN)_6]_2 \cdot xH_2O$ in a hot solution of CsCl
Zn_3Fe_2–C	$Zn_3[Fe(CN)_6]_2 \cdot xH_2O$	Precipitation from 0.01 M solutions of $K_3[Fe(CN)_6]$ and $ZnCl_2$ in 2:3 molar ratio
Zn_3Fe_2–H	$Zn_3[Fe(CN)_6]_2$	Hydrothermal treatment of Zn_3Fe_2–C in boiling water for 24 h and then excess of water evaporated at 80 °C up to dryness
Zn_3Co_2–C	$Zn_3[Co(CN)_6]_2 \cdot xH_2O$	Precipitation from 0.01 M solutions of $K_3[Co(CN)_6]$ and $ZnCl_2$ in 2:3 molar ratio
Zn_3Co_2–H	$Zn_3[Co(CN)_6]_2$	Hydrothermal treatment of Zn_3Co_2–C in boiling water for 24 h and then excess of water evaporated at 80 °C up to dryness
Zn_3Ir_2–C	$Zn_3[Ir(CN)_6]_2 \cdot xH_2O$	Precipitation from 0.01 M solutions of $K_3[Ir(CN)_6]$ and $ZnCl_2$ in 2:3 molar ratio
Zn_3Ir_2–H	$Zn_3[Ir(CN)_6]_2$	Hydrothermal treatment of Zn_3Ir_2–C in boiling water for 24 h and then excess of water evaporated at 80 °C up to dryness
Zn_3Cr_2–C	$Zn_3[Cr(CN)_6]_2 \cdot xH_2O$	Precipitation from 0.01 M solutions of $K_3[Cr(CN)_6]$ and $ZnCl_2$ in 2:3 molar ratio
Zn_3Mn_2–C	$Zn_3[Mn(CN)_6]_2 \cdot xH_2O$	Precipitation from 0.01 M solutions of $K_3[Mn(CN)_6]$ and $ZnCl_2$ in 2:3 molar ratio
ZnPt–C	$Zn[Pt(CN)_6]$	Precipitation from 0.01 M solutions of $K_2[Pt(CN)_6]$ and $ZnCl_2$ in 1:1 molar ratio

DicVol program [24]. The structural refinement from the obtained XRD powder patterns was carried out with the *Fullprof* 2005 code [25] and pseudo-Voigt peak shape lines. Peak profiles were calculated within 10 times the half linewidth. The background was modelled through third-order polynomial fitting.

3. Results and discussion

3.1. Classification of the studied samples according to the XRD powder pattern

According to the metals atomic ratio estimated from EDS analyses, for zinc hexacyanoferrates (II) formed in the presence of an alkaline ion, always mixed salts are obtained: $Zn_3A_2[Fe(CN)_6]_2 \cdot xH_2O$ (A = Na, K, Rb, Cs, NH_4). The mixed Zn–Cs ferrocyanide was also found as $ZnCs_2[Fe(CN)_6]$. This last composition was formed when the precipitation process was carried out in the presence of Cs^+. From ionic exchange always $Zn_3Cs_2[Fe(CN)_6]_2 \cdot xH_2O$ is obtained. For zinc hexacyanometallates (III) the estimated metals atomic ratio, close to 3:2, indicates formation of $Zn_3[M(CN)_6]_2 \cdot xH_2O$ (M = Cr, Mn, Fe, Co, Ir). In the studied samples, always a minor fraction of K was detected. For zinc hexacyanoplatinate (IV), the atomic ratio found corresponds to the following formula unit, $Zn[Pt(CN)_6] \cdot xH_2O$.

The obtained powders were classified according to the XRD powder pattern. For $Zn_3A_2[Fe(CN)_6]_2 \cdot xH_2O$ (A = Na, K, Rb, NH_4, Cs), it corresponds to a hexagonal cell (R-3c space group), which agrees with previous reports for A = Na, K, Cs [16–18]. $ZnCs_2[Fe(CN)_6]$ was found to be cubic (Fm-3m space group). This is the unit cell typical of Prussian blue analogues [15]. In this case, the framework metals (Fe, Zn) remain octahedrally coordinated to the ends of the bridge group (–C≡N–), while Cs^+ atoms remain filling all the interstitial voids. The estimated density for this cubic structure is 3.23 vs. 2.00 g/cm^3 for the hexagonal modification ($Zn_3Cs_2[Fe(CN)_6]_2 \cdot xH_2O$) (Table 2). For a bigger cation, for instance, tetra (methyl)ammonium $(TMA)^+$, such cubic structure is not formed and the ionic exchange from $Zn_3A_2[Fe(CN)_6]_2 \cdot xH_2O$ does not take place.

$Zn_3[M(CN)_6]_2 \cdot xH_2O$ (M = Fe, Co, Ir) were found to be dimorphic, cubic (Fm-3m) and hexagonal (R-3c). For iron,

Table 2
Hydration degree (water molecules per formula unit), unit cell parameters, calculated density and crystal structure refinement figures of merit for the studied zinc hexacyanometallates[a]

Sample	Hydration degree	Unit cell parameters (Å)	ρ_{Calc} (anhydrous) (g/cm^3)	Refinement figures of merit			
				R_{EXP}	R_{WP}	R_B	S
$Zn_3Na_2Fe_2$–H	8.9	$a = b = 12.4787(7)$ $c = 32.906(3)$	1.49	—	—	—	—
$Zn_3K_2Fe_2Fe_2$–H	6.8	$a = b = 12.5409(3)$ $c = 32.158(1)$	1.58	—	—	—	—
$Zn_3Rb_2Fe_2$–H	6.0	$a = b = 12.5013(2)$ $c = 32.512(1)$	1.79	6.23	9.83	10.26	1.58
$Zn_3(NH_4)2Fe_2$–H	9.3	$a = b = 12.5316(4)$ $c = 32.482(3)$	1.47	6.86	11.50	5.32	1.67
$ZnCs_2Fe$–C	0.0	$c = 10.3702(4)$	3.23	—	—	—	—
$Zn_3Cs_2Fe_2$–H	5.6	$a = b = 12.4841(3)$ $c = 32.832(4)$	2.00	—	—	—	—
Zn_3Fe_2–C	10.3	$c = 10.3392(1)$	1.22	—	—	—	—
Zn_3Fe_2–H	0.0	$a = b = 12.6011(2)$ $c = 32.971(9)$	1.36	6.64	10.24	9.25	1.54
Zn_3Co_2–C	11.6	$c = 10.2542(2)$	1.28	—	—	—	—
Zn_3Co_2–H	0.0	$a = b = 12.4847(3)$ $c = 32.756(1)$	1.41	5.47	8.93	9.00	1.63
Zn_3Ir_2–C	12.1	$c = 10.4821(3)$	1.71	—	—	—	—
Zn_3Ir_2–H	0.0	$a = b = 12.7752(5)$ $c = 33.595(2)$	1.87	—	—	—	—
Zn_3Cr_2–C	9.0	$a = 10.5826(1)$	1.13	—	—	—	—
Zn_3Mn_2–C	10.1	$a = 10.543(1)$	1.16	—	—	—	—
ZnPt–C	0.0	$c = 10.584(1)$	1.67	—	—	—	—

[a]The crystal structure for the hexagonal phase of the iridium compound was no refined.

this result confirms previous reports where this compound was reported as cubic (Fm-3m) [21] and also as hexagonal (R-3c) [19]. More recently it also appears reported as monoclinic [26,27], however, a detailed examination of the published XRD powder pattern interpreted as due to a monoclinic modification reveals that it really corresponds to the R-3c hexagonal phase. For zinc cobalticyanide, only a simple mention to the existence of the hexagonal phase was found [12]. The hexagonal structure of these zinc hexacyanometallates (III) corresponds to their high-temperature modification. When these hexacyanometallates (III) were prepared from hot solutions or the cubic phase was dehydrated by heating always the hexagonal structure was found. For intermediate temperatures, around 50 °C, usually a mixture of phases (hexagonal and cubic) is obtained.

For $Zn_3[M(CN)_6]_2 \cdot xH_2O$ (M = Cr, Mn), only the cubic cell (Fm-3m) was identified, even when the precipitate is obtained from hot solutions or when it was dehydrated by heating. In chromicyanides and manganicyanides, a relatively high charge delocalization on the metal linked to the N ends takes place [28]. Probably this fact could favour a relatively high stability for the zinc atom in an octahedral coordination. Zinc platinocyanide, $Zn[Pt(CN)_6]$, was also found to be cubic (Fm-3m), independently of the preparative route used. In its crystal structure, the two metal centres remain octahedrally coordinated to atoms from the bridge group (–C≡N–).

In Table 1, the studied samples appear labelled according to this classification, cubic (C) and hexagonal (H). The cubic phases were found to crystallize in the Fm-3m space group, typical of Prussian blue analogues [15], and the hexagonal ones in the R-3c space group. In the cubic phases, the two metal centres are found with an octahedral coordination. According to the 3:2 metals atomic ratio for zinc hexacyametallates (III), the crystal structure contains 33.33% of the $M(CN)_6$ sites vacant, creating a porous framework. These vacant sites force to a mixed coordination sphere for the Zn atom, $Zn(NC)_4(H_2O)_2$. Within the pores also zeolitic water molecules are accommodated, stabilized through hydrogen bonding interactions with the coordinated ones. In Table 2, the unit cell parameters calculated for all the studied samples are reported.

3.2. Thermo-gravimetry and thermal stability

Fig. 1 shows the TG curves for all the studied zinc ferrocyanides; and for zinc ferricyanide and cobalticyanide (both cubic and hexagonal). All the cubic zinc hexacyanometallates (III) show similar dehydration curves. The binding energy between coordinated water molecules and the zinc atom in these cubic hydrates has a minor contribution from the inner metal. The porous network allows an easy release of the water molecules evolved from the sample bulk. Zinc hexacyanoplatinate (IV) and hexagonal hexacyanometallates (III) were found to be

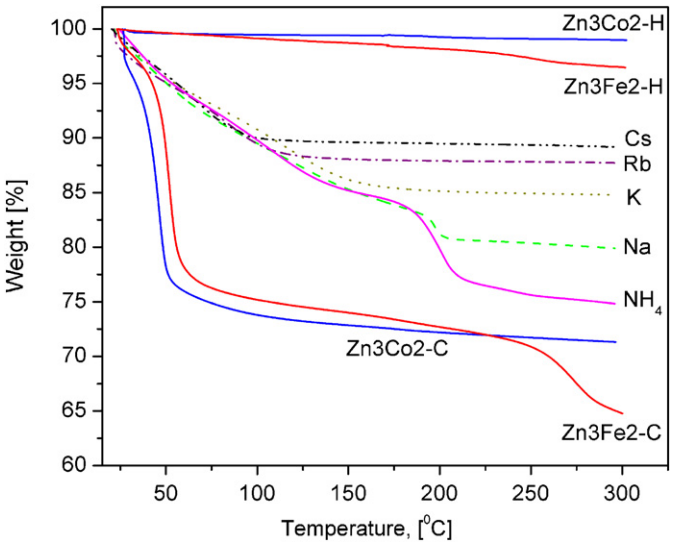

Fig. 1. Thermo-gravimetric curves (dehydration region only) for $Zn_3A_2Fe_2$–H (A = Na, K, Rb, Cs, NH_4); Zn_3Fe_2–C; Zn_3Co_2–C; Zn_3Fe_2–H and Zn_3Co_2–H.

anhydrous. These compounds have no available coordination sites for the stabilization of water molecules as coordinated species. It seems that their porous framework has insufficient polar character to allow the filling of the cavities system with non-coordinated waters. In Table 2, the hydration degree, estimated from the TG curves, for all the studied compounds, is reported. This table also contains the calculated densities (ρ, in g/cm^3) considering the obtained samples hydration degree and the unit cell parameters derived from the cell parameters refinement process (discussed later in the text).

The dehydration temperature for zinc ferrocyanides, taken at the end of the dehydration process, parallels the polarization power for the involved exchangeable cations. Within the pores these cations remain hydrated and those water molecules sited in their coordination sphere are the last ones to be released. The pores contain additional waters, of zeolitic nature, hydrogen bonded to the coordinated ones, probably forming water clusters. These weakly bonded water molecules abandon the solid at relatively low temperature in a practically continuous process. Once the first zeolitic waters are removed, the remaining ones enhance their mutual interactions and a higher temperature is required to allow their release. This could explain the observed form for the TG curves (Fig. 1). For zinc ammonium ferrocyanide, from about 150 °C an inflection in the TG curve was observed. Such inflection was taken as evidence of the ammonium molecule decomposition. It seems that the NH_4 decomposition and the evolution of the last coordinated water molecules take place simultaneously. Once dehydrated, zinc ferrocyanides remain stable up to 350 °C, which agrees with a previous report on the thermal stability for Zn–K ferrocyanide [1].

In cubic zinc hexacyanometallates (III), the water evolution also takes place through a continuous process but at lower temperature. The dehydration process usually ends before 60 °C, with a mass loss of about 30% of the sample weight. This corresponds to a relatively high hydration degree, from 10 to 12 water molecules per formula unit. Six of these water molecules are coordinated to zinc atoms, $ZnN_4(H_2O)_2$, and the remaining ones are hydrogen bonded to the coordinated ones. It seems that the loss of the most weakly bonded waters favours a stronger interaction between the remaining ones hindering a definite separation of their evolution in the TG curve. There is a wide temperature range, up to 225 °C in zinc ferricyanide, for instance, where the TG curve reveals a small but continuous weight loss. This behaviour was attributed to decomposition of small particles in the studied materials. Prussian blue analogues are usually obtained with relatively small particle size, with a sample fraction of practically colloidal nature. This fraction shows a higher instability on heating decomposing even at relatively low temperatures. Then, at higher temperature the sample decomposition as a whole takes place. This effect was observed in zinc ferricyanide above 200 °C to form a more stable ferrocyanide. Such decomposition reaction was confirmed from the IR spectra of the solid residues. On heating ferricyanides decompose liberating CN^- groups which play the role of reducing agent to give ferrocyanide plus C_2N_2 [29,30].

3.3. *Infrared and Mössbauer spectra of the studied zinc hexacyanometallates*

The IR spectra of hexacyanometallates are composed of three vibrations within the octahedral unit, $M(CN)_6$: ν(CN), δ(MCN) and ν(MC); and those motions from crystal water, ν(OH) and δ(HOH), when it is present [31]. In Table 3, the frequencies of these IR absorption bands for the studied solids are collected. Fig. 2 shows the ν(CN)

Table 3
Frequency (in cm^{-1}) of the IR absorption bands observed for the studied zinc hexacyanometallates

Sample	ν(CN)	δ(MCN)	ν(MC)	ν(OH)	δ(HOH)
$Zn_3Na_2Fe_2$–H	2101	606	493	3634, 3478	1614
$Zn_3K_2Fe_2$–H	2100	600	498	3631, 3502	1610
$Zn_3Rb_2Fe_2$–H	2101	603	496	3638, 3478	1610
$Zn_3(NH_4)2Fe_2$–H[a]	2099	606	490	3631, 3490	1609
$ZnCs_2Fe$–C	2092	594	450	—	—
$Zn_3Cs_2Fe_2$–H	2100	601	491	3629, 3452	1610
Zn_3Fe_2–C	2161, 2099	538	422	3645	1610
Zn_3Fe_2–H	2187, 2098	546	444	—	—
Zn_3Co_2–C	2189	—[b]	—[b]	3649, 3626	1612
Zn_3Co_2–H	2203	—[b]	—[b]	—	—
Zn_3Ir_2–C	2176	526	450	3656, 3430	1608
Zn_3Ir_2–H	2200	569	459	—	—
Zn_3Cr_2–C	2179	550	420	3550, 3390	1610
Zn_3Mn_2–C	2217	628	533	3540, 3350	1609
ZnPt–C	2230	511	414	—	—

[a] ν(NH) = 3155; δ(HNH) = 1442, 1404.
[b] The absorption band was not unequivocally assigned.

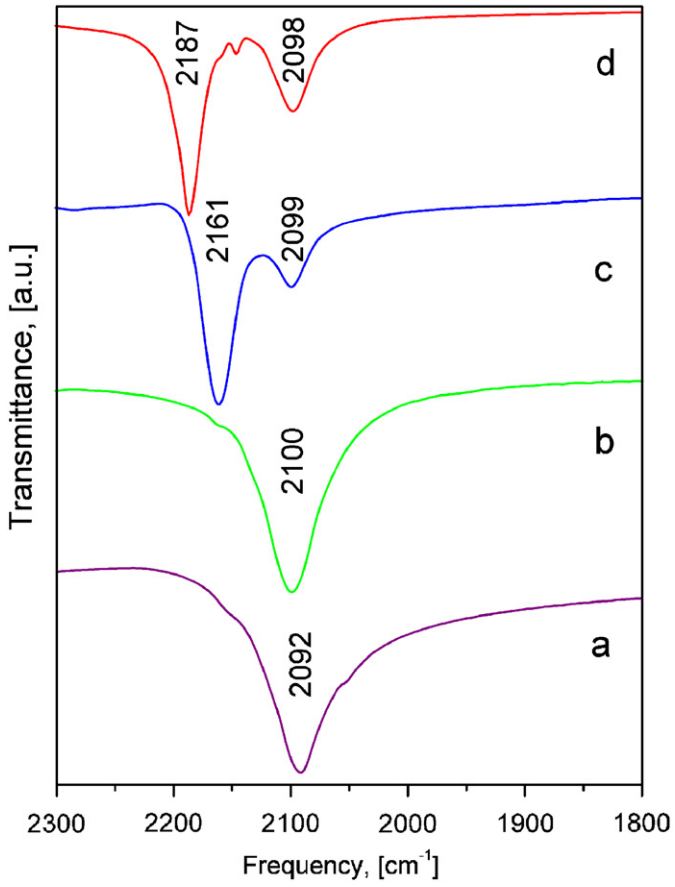

Fig. 2. ν(CN) vibration bands of dimorphic zinc hexacyanoferrates (II,III): (a) $ZnCs_2Fe$–C; (b) $Zn_3Cs_2Fe_2$–H; (c) Zn_3Fe_2–C; (d) Zn_3Fe_2–H. The CN stretching vibration is sensitive to the coordination number for the zinc atom. Zinc ferricyanides were obtained with impurities of Zn_3K2Fe_2–H.

absorption band for dimorphic zinc hexacyanoferrates (II,III). The ν(CN) band frequency is a good sensor for the valance, electronic configuration and coordination number of the metals bonded at the C and N ends of the CN ligands. For hexagonal zinc ferrocyanides, this vibration was observed around 2100 cm^{-1}, while it appears at 2092 cm^{-1} for cubic zinc–cesium ferrocyanide, a difference of 8 cm^{-1}. Between the cubic and hexagonal modifications of zinc ferricyanides such difference is even higher. The ν(CN) vibration in this compound was observed at 2187 and 2161 cm^{-1} for the hexagonal and cubic phase, respectively, a difference of 26 cm^{-1}. Between cubic and hexagonal zinc cobalticyanide, and iridicyanide this difference amounts to 14 and 24 cm^{-1}, respectively (Table 3). A decrease in the coordination number, from octahedral to tetrahedral, for instance, leads to an increase of the positive charge on the Zn atom, which, in turn, enhances the σ bonding [31]. This could explain the observed regularity of a higher ν(CN) absorption frequency for the hexagonal modification of the studied materials. The low-frequency vibrations, ν(MC) and δ(MCN), usually are of low intensity. The ν(MC) vibration appears also sensitive to the coordination number for the Zn atom. A reinforcement of the σ donation at the N end leads to a stronger M–C bond through an induced higher π^*-back donation at the C end, and to a higher frequency for the ν(MC) vibration. Between the cubic and hexagonal modifications for zinc ferricyanide and iridicyanide, such effect was observed as a frequency shift of 22 and 9 cm^{-1}, respectively (Table 3). The coordination number effect on the bending mode δ(MCN) must be less evident because it involves the motion of three atoms.

In the IR spectra of Zn_3Fe_2–H and Zn_3Fe_2–C, always a medium-intensity ν(CN) band due to $Zn_3K_2Fe_2$–H was observed. In ferrocyanides the ν(CN) band is very intense and broad, whereas in ferricyanide it is narrow and of medium intensity. From this fact, a small amount of ferrocyanide as impurity in a ferricyanide sample is sufficient to produce an intense ferrous band (Fig. 2). For instance, the observed ferrocyanide contribution in Fig. 2c,d was not detected by XRD (see the following text). According to the IR spectra of the prepared mechanical mixtures of Zn ferro- and ferri-cyanide, the ferrous fraction in the studied zinc ferricyanide samples remains below 5% by weight.

Within hexagonal zinc ferrocyanides, the charge balance cation (Na^+, K^+, Rb^+, $(NH_4)^+$, Cs^+) has a minor effect on the IR spectra. As already mentioned, these are exchangeable species which have a weak interaction with the material framework.

For zinc ferricyanide, the obtained Mössbauer spectrum is a quadrupole doublet of low-spin Fe(III) (Fig. 3, Table 4), which appears unresolved for the hexagonal phase ($\Delta = 0.18$ mm/s). Low-spin Fe(III) has five electrons in its t_{2g} orbitals. If these orbitals are non-equally populated by these five electrons, the iron nucleus senses the existence of an electric field gradient in its environment and a quadruple splitting interaction is detected in the obtained Mössbauer spectrum. An asymmetry for the iron atom ligands environment has the effect of producing the t_{2g} energy levels splitting and a non-symmetric distribution of these five electrons within the t_{2g} orbitals. In this sense, the quadrupole splitting value in low-spin Fe(III) serves as a sensor for the ligand symmetry around the iron atom. This low value of Δ (0.18 mm/s) for hexagonal zinc ferricyanide indicates that the energy splitting for the iron t_{2g} levels in this phase is of the order of kT at room temperature (k: Boltzmann constant, T: temperature in K). The thermal energy (kT) is sufficient to maintain these orbitals practically degenerated. It seems that during the assembling of the octahedral anionic block, $[Fe(CN)_6]^{n-}$, through the Zn atoms, to form the extended 3D framework, the octahedral symmetry around the iron atom is preserved. In the absence of unpaired electrons in the iron atom any quadrupole splitting interaction detected must be attributed to only the ligands environment. This could be the case of ferrocyanides. Mössbauer spectra of zinc ferrocyanides are single lines with a low isomer shift (δ) value, typical of low-spin Fe(II) (Fig. 3, Table 4). Such Mössbauer absorption signal, free of quadrupole splitting,

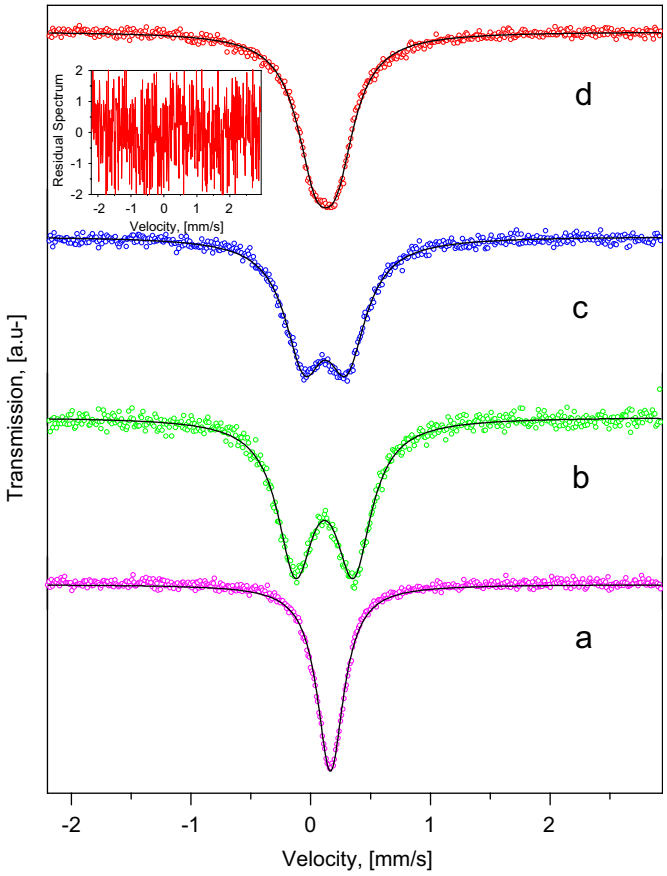

Fig. 3. Mössbauer spectra at room temperature for the studied zinc hexacyanoferrates (II,III): (a) $ZnCs_2Fe$–C; (b) Zn_3Fe_2–C (anhydrous); (c) Zn_3Fe_2–C (hydrate); (d) Zn_3Fe_2–H. *Inset*: Residual spectrum, in units of $\sigma(I_o)$ where I_o is the spectrum base line, for Zn_3Fe_2–H, which remains within $\pm 2\sigma$. Similar residual spectra were observed for all the studied zinc hexacyanoferrates (II,III).

Table 4
Mössbauer parameters at room temperature of the studied zinc hexacyanoferrates (II,III)

Compound	δ[a] (mm/s)	Δ (mm/s)	Γ (mm/s)	Assignment
$Zn_3Na_2Fe_2$–H	0.18	—	0.30	Low spin Fe(II)
$Zn_3K_2Fe_2$–H	0.18	—	0.26	Low spin Fe(II)
$Zn_3Rb_2Fe_2$–H	0.18	—	0.29	Low spin Fe(II)
$Zn_3(NH_4)2Fe_2$–H	0.18	—	0.37	Low spin Fe(II)
$ZnCs_2Fe$–C	0.18		0.31	Low spin Fe(II)
$Zn_3Cs_2Fe_2$–H	0.19	—	0.33	Low spin Fe(II)
Zn_3Fe_2–C hydrate	0.12	0.35	0.37	Low spin Fe(III)
Zn_3Fe_2–C anhydrous	0.11	0.49	0.42	Low spin Fe(III)
$Zn_3Zn_3Fe_2$–H	0.12	0.18	0.37	Low spin Fe(III)

[a]Values of δ are reported relative to sodium nitroprusside. Fitting error in the values of δ, Δ and Γ remains below 0.01 mm/s.

reveals the existence of a highly symmetric ligand environment around the iron atom. This is confirmed by the reported crystal structure for sodium–, potassium–, and cesium–zinc ferrocyanides [16–18] and by the crystal structures refined in the course of this study (discussed later).

The relatively large quadrupole splitting value observed for the cubic phase of zinc ferricyanide ($\Delta = 0.49$ mm/s) is closely related to the existence of vacant sites for the building block. The zinc atoms sited at surface of the cavity generated by a vacancy complete their octahedral coordination sphere with water molecules, in average $ZnN_4(H_2O)_2$. The CN group and the water molecule have different bonding properties, and from this fact the zinc atom must be out of its ideal symmetry restricted position (within the Fm-3m model) with a slightly deformed coordination environment. Since the metal centres (Fe, Zn) remain strongly linked through CN ligands certain local deformation is also generated around the iron atom and its environment becomes slightly asymmetric. Such local asymmetry around the iron atom produces a pronounced energy splitting for its t_{2g} orbitals and an asymmetric distribution of the 3d electrons (five) within these orbitals. This effect is the main responsible for the relatively large Δ value observed for the cubic phase of this compound. Certain contribution to the value of Δ also proceeds from an asymmetric π-back donation [32]. In porous Prussian analogues the vacant sites are randomly distributed. Related to this feature, the Mössbauer spectra of ferricyanides appear to be doublets formed by broaden lines. These spectra can be interpreted as a distribution of quadrupole splitting (Δ) values [3]. However, such distribution has a symmetric shape and from the spectra fitting according to a single doublet the average values for isomer shift (δ) and quadrupole splitting (Δ) can be obtained. In this sense, the Mössbauer parameters reported in Table 4 for cubic zinc ferricyanide in its hydrated and anhydrous forms must be taken as average values.

The observed zinc ferrocyanide fraction in the IR spectra of the zinc ferricyanide samples, both in cubic and hexagonal modifications (Fig. 2), was appreciated in the corresponding Mössbauer spectra as a slight asymmetry for the observed quadrupole splitting doublet (Fig. 3). The ferric and ferrous species have slightly different isomer shift values (Table 4) and this originates that asymmetry. According to the signals intensities, such ferrous contribution was estimated to be about 2% of the sample weight or perhaps slightly higher because these signals appear with a strong overlapping. IR spectra suggest up to 5% of ferrous contribution and in XRD it is not detected.

The low-spin configuration for both iron (II) and iron(III) results from a very strong interaction of the iron atom with the CN ligands at the C ends. The CN group has a low-energy π^*-antibonding orbital at its C end which is used to abstract electrons from the iron d_{xy}, d_{xz}, and d_{yz} orbitals. This π-back bonding interaction leads to a significant reduction for the 3d electrons shielding effect on the s-electron density at the iron nucleus which explains the extremely low δ value observed. The π^*-back bonding interaction is more intense for iron(II) due to the higher availability of electrons in t_{2g} orbitals. As already mentioned, the exchangeable cation has a weak interaction

with the material framework and from this fact, it has practically no effect on the value of δ.

3.4. Behaviour of cubic zinc hexacyanometallates (III) on dehydration

As already discussed, for dimorphic hexacyanometallates (III), $Zn_3[M(CN)_6]_2$ (M = Fe, Co, Ir), the precipitated cubic phase appears as hydrate, while the hexagonal modification obtained by heating of such hydrated phase results anhydrous. In the cubic structure, the coordination environment for the Zn atom is formed by four N atoms from –NC ligands plus two water molecules. This could suggest that the structural transformation, from cubic into hexagonal, could be induced by removal of the coordinated water molecules. However, the cubic phase can be dehydrated at room temperature under vacuum preserving the Fm-3m crystal structure. When XRD powder patterns were recorded within a vacuum camera (10^{-5} Torr), a peak shift to higher values of 2θ, indicating the occurrence of a cell contraction on dehydration (Fig. 4), was observed. In this soft dehydration process only the formation of a minor fraction of the hexagonal phase was detected (Fig. 4, inset). In Table 5, the calculated cell contraction on dehydration for zinc ferri- and cobalti-cyanides is collected. The weight loss related to the vacuum dehydration at room temperature was similar to that estimated from the TG curves. Since in this soft dehydration process the coordinated waters are also removed, in the anhydrous cubic material, the zinc atom remains coordinated to only four N atoms, probably adopting a local pseudo-tetrahedral coordination. When the anhydrous cubic sample was heated a progressive structural transformation with formation of the hexagonal phase was observed. It seems that the thermal energy (kT) contributes to overcome the energy barrier between such pseudo-tetrahedral coordination and the tetrahedral one favouring the phase transformation, from cubic into hexagonal. The anhydrous cubic phase shows a hydrophilic behaviour through the ability of the Zn atom to incorporate water to its coordination environment in order to restore the octahedral coordination. As already mentioned, for the hexagonal modification this behaviour was not observed and the porous solid remains as hydrophobic for at least a week in humid air. The inverse transformation is only observed when the hexagonal phase is exposed several days, at room temperature, to humid air. XRD powder patterns of these two anhydrous phases (cubic and hexagonal) were also recorded at 77 K (under vacuum). On cooling the cell contraction was observed. For the cubic phase the cell volume reduction was about 4%, however, for the hexagonal one it hardly amounts 0.4% (Table 5). The hexagonal R-3c cell, where both metal centres have saturated their coordination spheres with atoms from the framework, appears with a particularly high rigidity. The tetrahedral coordination for the zinc atom leads to the formation of a more dense and robust structure.

The Mössbauer spectrum is particularly sensitive to the water molecules removal from the cubic phase. As already mentioned, at the pore surface six Zn atoms are found,

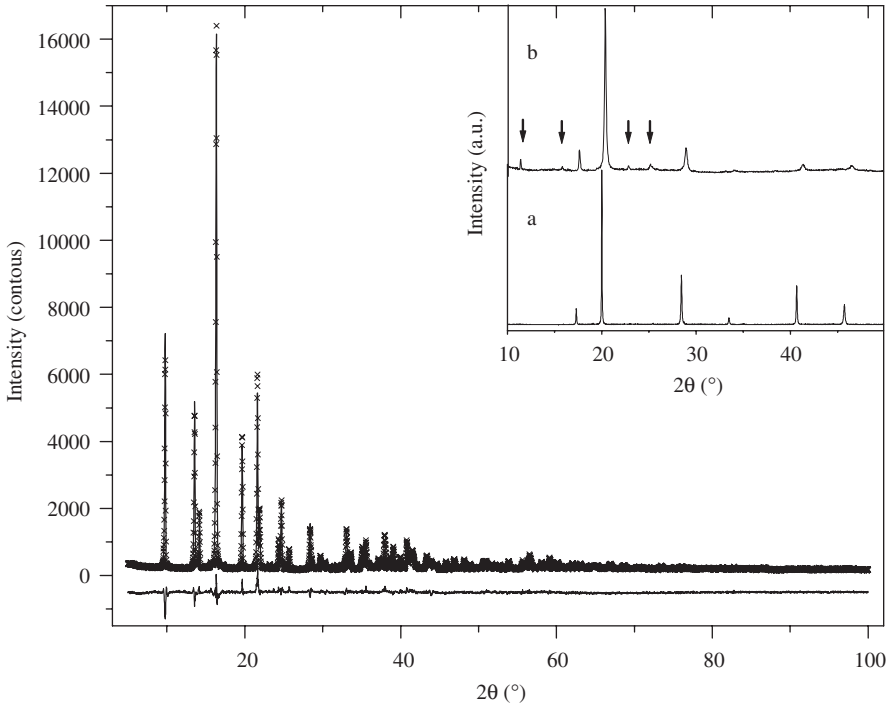

Fig. 4. XRD powder pattern, experimental, calculated and their difference of Zn_3Co_2–H. *Inset*: (a) Zn_3Co_2–C hydrate (cubic Fm-3m cell); (b) Zn_3Co_2–C dehydrated under vacuum at room temperature. On the water removal, a cell contraction is observed but preserving the cubic unit cell. The formation of a small fraction of the hexagonal phase (Zn_3Co_2–H), indicated by arrows, is also detected.

Table 5
Cell contraction, estimated from XRD powder patterns recorded at 300 and 77 K under vacuum, for the cubic phases of zinc ferri- and cobalti-cyanides on dehydration

Sample	Under vacuum at 300 K		Under vacuum at 77 K		Under vacuum at 77 K	
	Cell[a] contraction (Å)	Volume[a] reduction (%)	Cell[b] contraction (Å)	Volume[b] reduction (%)	Cell[c] contraction (Å)	Volume[c] reduction (%)
Zn_3Fe_2–C	0.161(2)	4.6	0.146(2)	4.2	$a=b=0.006(3)$ $c:<0.001$	<0.4
Zn_3Co_2–C	0.197(1)	5.6	0.181(1)	5.2	$a=b=0.003(3)$ $c:<0.001$	<0.4

[a]Cubic phase, related to the hydrated form at 300 K.
[b]Cubic phase, related to the anhydrous form at 300 K.
[c]Hexagonal phase, related to the unit cell parameters at 300 K.

with a mixed coordination sphere, $Zn(NC)_4(H_2O)_2$. When these coordinated waters are removed, and even the zeolitic ones, the Zn atom interaction with the CN ligand changes and it is sensed at the iron site [32]. In the anhydrous state the zinc atom remains coordinated to only four N ends and all the bonding interaction is with the CN groups. This leads to a higher charge subtraction from these groups, via σ-bonding (through 5σ orbitals), which induces a higher and asymmetrical π-back bonding interaction with the iron atom. The net effect is a more asymmetric charge environment around the iron nucleus which is observed as a higher Δ value and at the same time, a slight reduction in the isomer shift value (Fig. 3b, Table 4). This bond strengthening between the metal centres through the CN ligand in the anhydrous cubic sample correlates with the observed cell contraction on the crystal water removal (Fig. 4, inset; Table 5) and also with the reported effect of the adsorbed water on the magnetic properties of Prussian blue analogues [32].

3.5. Crystal structures refinement

Of the studied family of zinc hexacyanometallates, eight compositions were found to be hexagonal (R-3c space group). For three of them (Zn–Na, Zn–K, Zn–Cs), the crystal structures have been reported [16–18]. For Zn hexacyanoiridate (III), the XRD powder pattern obtained was of insufficient quality to be used in a crystal structure refinement process. For the remaining four compositions, Zn–Rb and Zn–NH_4 ferrocyanides and Zn ferri- and cobalti-cyanides, the crystal structures were refined using the Rietveld method. As starting structural model to be refined, the reported structure for $Zn_3K_2[Fe(CN)_6]_2 \cdot xH_2O$ [16] was taken. This structure provided the initial positions for the framework atoms. The interatomic C–N distance was constrained to take values within certain limits considering results from single crystal studies in analogue compositions [16–18,21]. In Table 6, the crystallographic positions where the atoms are sited appears indicated.

Table 6
Atomic positions and temperature (Biso) and occupation (Occ) factors for the refined crystal structures (hexagonal R-3c)

Sample and atoms	Site	x	y	z	Biso	Occ
Zn_3Co_2–H						
Co	12(c)	0	0	0.1473(1)	2.4(1)	0.3333
Zn	18(e)	0.2902(2)	0	0.25	3.15(7)	0.5
C1	36(f)	0.1175(9)	−0.016(1)	0.1798(3)	3.0(2)	1.0
N1	36(f)	0.1807(7)	−0.027(1)	0.2031(2)	3.0(2)	1.0
C2	36(f)	0.1272(8)	0.1149(9)	0.1125(3)	3.0(2)	1.0
N2	36(f)	0.2144(6)	0.1892(7)	0.0963(3)	3.0(2)	1.0
Zn_3Fe_2–H						
Fe	12(c)	0	0	0.1466(6)	1.75(1)	0.3333
Zn	18(e)	0.2900(3)	0	0.25	2.48(7)	0.5
C1	36(f)	0.1159(4)	−0.015(2)	0.1797(9)	1.85(7)	1.0
N1	36(f)	0.1811(2)	−0.023(3)	0.2028(1)	1.85(7)	1.0
C2	36(f)	0.1302(1)	0.1161(10)	0.1133(5)	1.85(7)	1.0
N2	36(f)	0.2163(1)	0.1906(11)	0.0969(2)	1.85(7)	1.0
$Zn_3Rb_2Fe_2$–H						
Fe	12(c)	0	0	0.1466(8)	1.72(6)	0.3333
Zn	18(e)	0.2883(6)	0	0.25	2.23(3)	0.5
C1	36(f)	0.1090(6)	−0.0159(9)	0.1837(2)	1.95(2)	1.0
N1	36(f)	0.1752(4)	−0.034(1)	0.2026(3)	1.95(2)	1.0
C2	36(f)	0.1396(4)	0.114(4)	0.1156(6)	1.95(2)	1.0
N2	36(f)	0.2145(4)	0.191(2)	0.0960(9)	1.95(2)	1.0
Rb	36(f)	0.4433(2)	0.1407(10)	0.3582(3)	10.3(4)	0.32(3)
O1	36(f)	0.2597(7)	0.296(7)	0.2834(2)	11.8(5)	0.26(8)
O2	36(f)	0.5325(9)	0.249(2)	0.3485(3)	11.8(5)	0.39(6)
O3	36(f)	0.3513(1)	0.389(1)	0.2137(3)	11.8(5)	0.18(7)
$Zn_3(NH_4)2Fe_2$–H						
Fe	12(c)	0	0	0.1470(1)	2.22(9)	0.3333
Zn	18(e)	0.2905(2)	0	0.25	3.15(7)	0.5
C1	36(f)	0.1114(9)	−0.0212(11)	0.1811(3)	2.7(2)	1.0
N1	36(f)	0.1809(7)	−0.0262(10)	0.2030(2)	2.7(2)	1.0
C2	36(f)	0.1337(8)	0.1159(9)	0.1143(3)	2.7(2)	1.0
N2	36(f)	0.2156(6)	0.1886(6)	0.0957(3)	2.7(2)	1.0
NH_4	36(f)	0.557(8)	0.386(5)	0.3155(10)	10.8(1)	0.34(9)
O1	36(f)	0.454(12)	0.112(13)	0.355(3)	12.05(8)	0.39(8)
O2	36(f)	0.298(6)	0.308(5)	0.2799(10)	12.05(8)	0.54(6)
O3	36(f)	0.511(8)	0.499(9)	0.309(2)	12.05(8)	0.21(2)
O4	36(f)	0.392(13)	0.355(7)	0.291(2)	12.05(8)	0.45(6)

The reported errors are those derived from the refinement cycles; the expected uncertainty in the given atomic positions is probably higher.

In this structural model the C and N atoms sites have unitary occupation while it is 0.5 and 0.333 (1/3) for Zn and the inner metal, respectively. The charge balancing cation and the water molecules are extra-framework species sited within the pores. These species, and also the C and N atoms, are sited in the general 36(f) positions. Within this structural model the crystal structures of these phases were refined with excellent patterns fitting (small S value) and satisfactory refinement figures of merit (R_{WP} and R_B) (Table 2). The refined atomic positions and thermal and occupation factors are reported in Table 6, while in Table 7 the interatomic distances and bond angles are collected. Fig. 4 shows the experimental and the fitted XRD powder patterns for Zn cobalticyanide. In Fig. 5 (left), the coordination environment for the metal centres and the atomic packing within the unit cell (right) are shown.

The crystal structure of the studied hexagonal Zn compounds can be considered as the assembly of MC_6 octahedra and ZnN_4 tetrahedra to form a porous 3D framework (Fig. 6). It can also be regarded as $M(CN)_6$ octahedral blocks bridged by Zn atoms bonded at their N ends through a tetrahedral coordination with these binding sites. According to the bond angles (Table 7) during the zinc salt formation the building unit, $[M(CN)_6]$, approximately preserves its original geometry. However, the N–Zn–N bonds deviates from the linearity, with an average angle of about 108°. Slightly different Zn–N interatomic distances are observed from the refined crystal structures indicating that the tetrahedron around the Zn atom is distorted (Table 6). This feature and the difference of coordination number for the involved metal centres lead to formation of relatively large ellipsoidal cavities *ca.* $15 \times 9 \times 8$ Å, which remain communicated by elliptical openings (windows) of about 6 Å of larger diameter (Fig. 6). At the surface of a given cavity eight octahedra and twelve tetrahedra are found and since these building units are shared with a neighbouring cavity, the amount of formula units per cavity is two. For the cubic phase (Fm-3m space group), the N–Zn–N angle is close to 90°, and the cavity can be described as a sphere.

The tetrahedral coordination leads to a particularly strong bond of the CN ligand with the Zn atom. For instance, the estimated Zn–N distance for hexagonal zinc ferricyanide (Table 7) is about 0.1 Å shorter than the corresponding value reported for the cubic analogue, which is 2.094 Å [21]. This evidence is also supported by the IR spectroscopy data, where the higher values for the frequency of ν(CN) and ν(MC) vibrations were observed for the hexagonal structure.

Table 7
Bond distances (in Å) and bond angles (in deg) for the refined structures

Sample	Bond distances (Å)		Bond angles (deg)	
Zn_3Co_2–H	Co–C1 = 1.903(2)	Zn–N1 = 1.973(5)	C1–Co–C1″ = 88.9(9)	N1–Zn–N1′ = 96.3(9)
	Co–C2 = 1.898(6)	Zn–N2 = 1.965(1)	C1–Co–C2 = 88.9(4)	N1–Zn–N2′ = 102.5(8)
	C1–N1 = 1.154(3)	C2–N2 = 1.147(6)	C1–Co–C2′ = 175.8(6)	N2–Zn–N2′ = 110.6(10)
			C2–Co–C2′ = 87.6(4)	N2–Zn–N1 = 122.7(6)
			C2–Co–C1′ = 94.5(6)	Zn–N1–C1 = 162.3(8)
			Co–C1–N1 = 171.8(6)	Zn–N2–C2 = 164.9(3)
			Co–C2–N2 = 170.2(3)	
Zn_3Fe_2–H	Fe–C1 = 1.910(1)	Zn–N1 = 1.997(3)	C1–Fe–C1′ = 90.5(3)	N1–Zn–N1′ = 104.3(10)
	Fe–C2 = 1.908(4)	Zn–N2 = 1.971(7)	C1–Fe–C2 = 89.9(2)	N1–Zn–N2′ = 105.8(5)
	C1–N1 = 1.160(3)	C2–N2 = 1.155(3)	C1–Fe–C2′ = 179.5(5)	N2–Zn–N2′ = 110.6(2)
			C2–Fe–C2′ = 90.1(6)	N2–Zn–N1 = 115.1(7)
			C2–Fe–C1′ = 89.3(9)	Zn–N1–C1 = 164.1(1)
			Fe–C1–N1 = 174.0(1)	Zn–N2–C2 = 165.1(2)
			Fe–C2–N2 = 172.7(2)	
$Zn_3Rb_2Fe_2$–H	Fe–C1 = 1.903(2)	Zn–N1 = 1.985(2)	C1–Fe–C1′ = 84.2(10)	N1–Zn–N1′ = 105.9(6)
	Fe–C2 = 1.901(1)	Zn–N2 = 1.966(4)	C1–Fe–C2 = 92.2(2)	N1–Zn–N2′ = 109.9(4)
	C1–N1 = 1.147(5)	C2–N2 = 1.146(3)	C1–Fe–C2′ = 172.3(7)	N2–Zn–N2′ = 107.4(7)
			C2–Fe–C2′ = 94.4(5)	N2–Zn–N1 = 111.8(10)
			C2–Fe–C1′ = 88.7(5)	Zn–N1–C1 = 151.4(5)
			Fe–C1–N1 = 171.8(5)	Zn–N2–C2 = 156.9(5)
			Fe–C2–N2 = 170.2(1)	
$Zn_3(NH_4)2Fe_2$–H	Fe–C1 = 1.904(3)	Zn–N1 = 1.968(5)	C1–Fe–C1′ = 89.4(7)	N1–Zn–N1′ = 104.2(1)
	Fe–C2 = 1.900(2)	Zn–N2 = 1.962(3)	C1–Fe–C2 = 90.2(3)	N1–Zn–N2′ = 107.6(2)
	C1–N1 = 1.148(4)	C2–N2 = 1.147(5)	C1–Fe–C2′ = 177.8(7)	N2–Zn–N2′ = 112.9(1)
			C2–Fe–C2′ = 91.8(8)	N2–Zn–N1 = 111.4(4)
			C2–Fe–C1′ = 88.4(1)	Zn–N1–C1 = 162.6(5)
			Fe–C1–N1 = 175.1(9)	Zn–N2–C2 = 159.9(1)
			Fe–C2–N2 = 177.7(8)	

The reported errors are those derived from the refinement cycles; the expected uncertainty in the interatomic distances is probably higher.

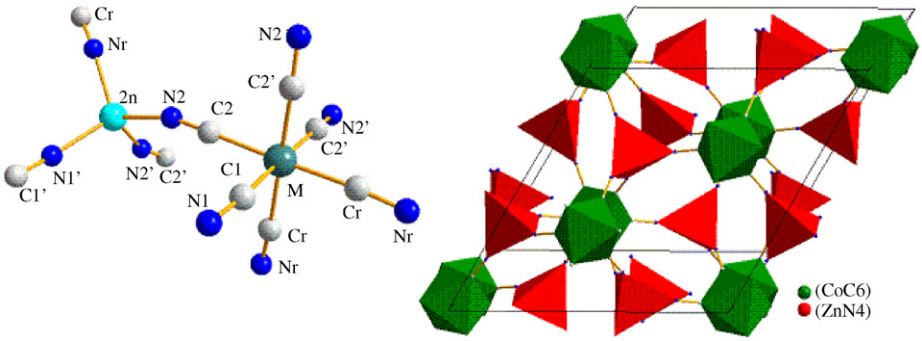

Fig. 5. *Left*: Coordination environment for the metal centres. *Right*: Unit cell of hexagonal zinc hexacyanometallates.

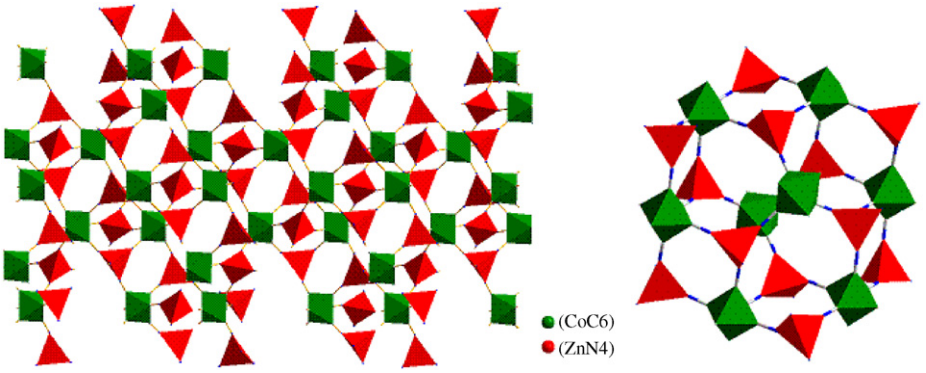

Fig. 6. *Left*: Porous framework of hexagonal zinc hexacyanometallates formed as the assembling of octahedra, MC_6 and tetrahedra, ZnN_4. Relativity large ellipsoidal cavities remain communicated by elliptical windows. *Right*: An isolated cavity where at the surface eight MC_6 octahedra and 12 ZnN_4 tetrahedra are observed.

In the mixed zinc ferrocyanides, the water molecules appear in the charge balancing species environment, a fraction of them in its coordination sphere. In the absence of that species (A^+) the porous framework results anhydrous. The coordinated waters serve as adsorption sites to stabilize additional water molecules through hydrogen bond interactions. These extra-framework species (A^+ and H_2O) have a relative high isotropic factor of thermal agitation (Table 6), suggesting that they have a relatively weak interaction with the material framework. For zinc hexacyanoferrates (II) the twelve available exchangeable cations per cell could be sited close to the cavity windows. From an electrostatic point of view, the A^+ cation must be sited in the cavity region of higher electric field gradient, probably close to the pore windows. The estimated coordinates for these weakly bonded species can be considered as average values.

3.6. Magnetic interaction

Of the zinc hexacyanometallates that are considered in this study, only for Cr(III), Mn(III) and Fe(III) analogues certain magnetic order is expected, and of them only the iron compound appears dimorphic. The study of the magnetic properties was limited to zinc ferricyanide in order to shed light on a probable structural effect on the magnetic interaction and also to obtain information on the role of the polymeric structure in the cooperative magnetic ordering.

The magnetic interaction in zinc ferricyanide arises from atoms with identical electronic configuration, ($Fe(III)t_{2g}^5$, $S = 1/2$). From this fact the magnetic ordering, when it is established, must be of anti-ferromagnetic nature. The reciprocal mass susceptibility ($1/\chi_p$) as a function of the temperature (T) is shown in Fig. 7. In the 15–40 K temperature region, this curve shows a linear dependence and it was fitted according to the Curie–Weiss law, $\chi^{-1} = (T-\theta_{CW})/C$, to derivate the Curie constant C and Curie–Weiss temperature $|\theta_{CW}|$. The estimated θ_{CW} values are $-5.1(1)$ K and $-3.7(1)$ K for cubic and hexagonal zinc ferricyanide, respectively. The corresponding Curie constant value results 0.018(1) K (cubic phase) and 0.022(1) K (hexagonal phase). The negative sign of θ_{CW} corresponds to an anti-ferromagnetic interaction. The weaker interaction for the hexagonal phase where the iron atoms appear at a distance of 7.4 Å between them, versus 10.2 Å in the cubic structure, was attributed to the non-linear character of the Fe–C≡N–Zn–N≡C–Fe interaction path. This is related to the tetrahedral coordination for the zinc atom where the N–Zn–N angle in average is 108°. In the cubic phase, this interaction path lies on practically a straight line, favouring the unpaired electrons spin coupling from

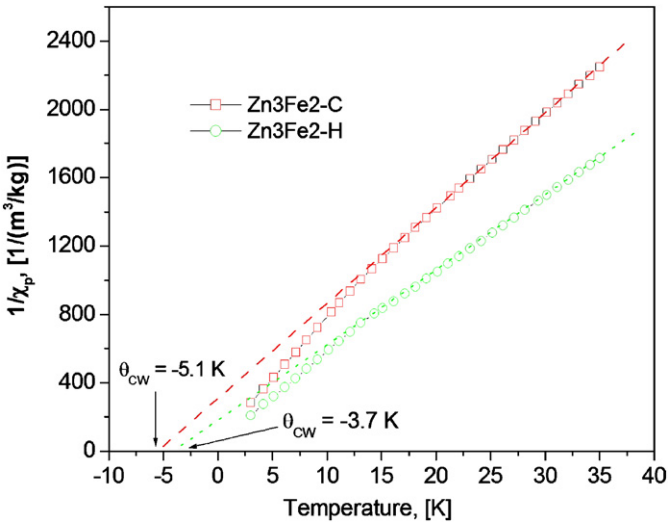

Fig. 7. Reciprocal mass susceptibility ($1/\chi_p$) as a function of temperature for zinc ferricyanide, in both cubic and hexagonal phase. Indicated is the estimated value for the Curie–Weiss constant, θ_{CW}.

neighbouring iron atoms. Below 15 K, the $1/\chi_p$ vs. T curve shows an inflection. However, the nature of that inflection cannot be unequivocally interpreted with available data.

The relative strong magnetic interaction between distant iron(III) atoms in zinc ferricyanide is possible due to the charge delocalization through the CN bridges. In potassium ferricyanide without such effective interaction path, the cooperative anti-ferromagnetic interaction is only detected below 0.2 K [33]. This is an expected behaviour. The relatively high temperature of magnetic order for Prussian blue analogues-based molecular magnets, in some of them above room temperature [34], are possible by the role of the $-C\equiv N-$ bridges to allow a high overlapping density between unpaired electrons from neighbouring metal centres.

4. Conclusions

Zinc hexacyanometallates were explored in order to identify those compositions where the zinc atom appears tetrahedrally coordinated to the N end of CN ligands. Such coordination was found in the family $Zn_3A_2[Fe(CN)_6]_2 \cdot xH_2O$ (A = Na, K, Rb, Cs, NH_4) and also in $Zn_3[M(CN)_6]_2$ (M = Fe, Co, Ir). These last three compositions were found to be dimorphic, cubic (Fm-3m) and hexagonal (R-3c), related to Zn atom in octahedral and tetrahedral coordination, respectively. The mixed Zn–Cs hexacyanoferrates (II) was also found dimorphic but with two different formula unit. The cubic modification corresponds to $ZnCs_2[Fe(CN)_6]$ where both Zn and Fe are octahedrally coordinated to the CN bridge forming a cubic framework with the Cs atoms occupying all the interstitial positions. The crystal structures of $Zn_3A_2[Fe(CN)_6]_2 \cdot xH_2O$ (A = Rb, NH_4) and $Zn_3[M(CN)_6]_2$ (M = Fe, Co) (hexagonal phases) were refined from XRD powder patterns in the R-3c space group reported for $Zn_3K_2[Fe(CN)_6]_2 \cdot xH_2O$. The IR spectrum, through the ν(CN) and ν(MC) vibrations, appears as an excellent sensor to identify the coordination number for the Zn atom in a given sample within the studied family of materials. The tetrahedral coordination is always related to a relatively high frequency for the ν(CN) and ν(MC) absorption bands. In the absence of an exchangeable (extra-framework) cation (A), the hexagonal phases appear to be an anhydrous material, which was ascribed to a low polar character for the pore surface. For the hydrated phases, the crystal water can be removed without disrupting the porous structure. The resulting anhydrous material remains stable up to above 250 °C.

Acknowledgements

This study was partially supported by CONACyT (Mexico) through the cooperation project J200.813, and also from the project SEP-2004-C01-47070. R.M.G. thanks the support provided by CLAF-ICTP for his Ph.D. studies. The authors thank LNLS (Campinas, Brazil) the access to the synchrotron radiation facility. The help of E. Fregoso-Israel from IIM-UNAM for the TG data acquisition is acknowledged.

References

[1] P. Cartraud, A. Cointot, A. Renaud, J. Chem. Soc. Faraday Trans. 1 (77) (1981) 1561.
[2] M.V. Bennet, L.G. Beauvais, M.P. Shores, J.R. Long, J. Am. Chem. Soc. 123 (2001) 8022.
[3] J. Balmaseda, E. Reguera, A. Gomez, B. Diaz, A. Autie, Microporous Mesoporous Mater. 54 (2002) 285.
[4] J. Balmaseda, E. Reguera, J. Rodríguez-Hernández, L. Reguera, M. Autie, Microporous Mesoporous Mater. 96 (2006) 222.
[5] J. Roque, E. Reguera, J. Balmaseda, J. Rodríguez-Hernández, L. Reguera, L.F. del Castillo, Microporous Mesoporous Mater. (2007).
[6] S.S. Kaye, J.R. Long, J. Am. Chem. Soc. 127 (2005) 6506.
[7] K.W. Chapman, P.D. Southon, C.L. Weeks, C.J. Kepert, Chem. Commun. (2005) 3322.
[8] M.R. Hartman, V.K. Peterson, Y. Liu, S.S. Kaye, J.R. Long, Mater. Chem. 18 (2006) 3221.
[9] S.S. Kaye, J.R. Long, Catal. Today (2006).
[10] G. Boxhoorn, J. Moolhuysen, J.P.G. Coolegem, R.A. van Santen, J. Chem. Soc. Chem. Commun. (1985) 1305.
[11] S. Ayrault, B. Jimenez, E. Garnier, M. Fedoroff, D.J. Jones, C. loss-Neskovich, J. Solid State Chem. 141 (1998) 475.
[12] J. Kuyper, G. Boxhoorn, J. Catal. 105 (1987) 163.
[13] E. Reguera, J. Fernandez, C. Diaz, J. Molerio, Hyperfine Interact. 73 (1992) 285.
[14] L. Roberts, Science 238 (1987) 1028.
[15] A. Ludi, H.U. Gudel, Struct. Bond. 14 (1973) 1.
[16] P. Gravereau, E. Garnier, A. Hardy, Acta Crystallogr. B 35 (1979) 2843.
[17] P. Gravereau, E. Garnier, A. Hardy, Acta Crystallogr. B 38 (1982) 1401.
[18] E. Garnier, P. Gravereau, Rev. Chim. Mineral. 20 (1983) 68.
[19] E. Garnier, P. Gravereau, K. Ahmadi, A. Hardy, Rev. Chim. Mineral. 21 (1984) 144.
[20] G. Brauer, Handbook of Preparative Inorganic Chemistry, second ed., vol. 2, Academic Press, New York, 1965, p. 1373.
[21] E. Garnier, P. Gravereau, Acta Crystallogr. C 40 (1984) 1306.

[22] J. Fernandez, E. Reguera, Solid State Ionics 93 (1996) 139.
[23] Z. Klencsar, Mosswinn Program, Budapest 2001. 〈http://www.mosswinn.com/〉.
[24] D. Louer, R. Vargas, J. Appl. Crystallogr. 15 (1982) 542.
[25] J. Rodriguez-Carvajal, FullProf 2005 Program, Institute Louis Brillouin, Saclay, France, 2005.
[26] C.W. Ng, J. Ding, L.M. Gan, J. Phys. D 34 (2001) 1188.
[27] J. Ding, C.W. Ng, Y. Shi, IEEE Trans. Magn. 37 (2001) 2935.
[28] T. Mallah, S. Thiébaut, M. Verdaguer, P. Veillet, Science 262 (1993) 1554.
[29] E. Reguera, J. Fernández, J. Balmaseda, Transition Met. Chem. 24 (1999) 648.
[30] E. Reguera, J. Balmaseda, G. Quintana, J. Fernandez, Polyhedron 17 (1998) 2353.
[31] K. Nakamoto, Infrared and Raman Spectra of Inorganic and Coordination Complexes, Wiley, New York, 1986.
[32] R. Martinez-Garcia, M. Knobel, E. Reguera, J. Phys.: Condens. Matter 18 (2006) 11243.
[33] J.J. Fritz, J. Cesarano, T. Goto, J. Chem. Phys. 65 (1976) 134.
[34] S.M. Holmes, G.S. Girolami, J. Am. Chem. Soc. 121 (1999) 5593.